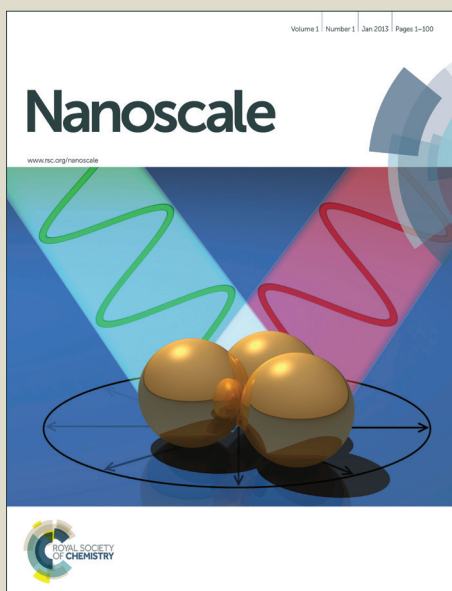


Nanoscale

Accepted Manuscript



This is an *Accepted Manuscript*, which has been through the Royal Society of Chemistry peer review process and has been accepted for publication.

Accepted Manuscripts are published online shortly after acceptance, before technical editing, formatting and proof reading. Using this free service, authors can make their results available to the community, in citable form, before we publish the edited article. We will replace this *Accepted Manuscript* with the edited and formatted *Advance Article* as soon as it is available.

You can find more information about *Accepted Manuscripts* in the [Information for Authors](#).

Please note that technical editing may introduce minor changes to the text and/or graphics, which may alter content. The journal's standard [Terms & Conditions](#) and the [Ethical guidelines](#) still apply. In no event shall the Royal Society of Chemistry be held responsible for any errors or omissions in this *Accepted Manuscript* or any consequences arising from the use of any information it contains.



Journal Name

ARTICLE

Preparation, Optical and Electrical Properties of PTCDA Nanostructures

Yuyan Han,^a Wei Ning,^a Haifeng Du,^a Jiyong Yang,^a Ning Wang,^a Liang Cao,^a Feng Li,^a Fapei Zhang,^a Faqiang Xu^{*,b} and Mingliang Tian^{*,a}

Film, nanorods (NRs), nanowires (NWs), and nanoparticles (NPs) of perylene-3,4,9,10-tetracarboxylic dianhydride (PTCDA) were prepared by organic molecular beam deposition (OMBD) on porous anodic alumina oxide (AAO) at different substrate temperatures (T_s). The scanning electron microscopy (SEM) study shows that the morphologies of the nanostructures (NS) formed on AAO strongly depend on the T_s . The absorption spectra of different PTCDA NS present the strong absorbance in the wavelength range of 400~600 nm, and the photoluminescence (PL) spectra show blue shift as T_s increases. The current versus voltage (I - V) characteristic illustrates that the electrical conductivity of the single-crystal NW is about $3 \pm 0.1 \text{ S}\cdot\text{m}^{-1}$ which is much higher than the conductivity of PTCDA film reported previously.

Received 00th January 20xx,
Accepted 00th January 20xx

DOI: 10.1039/x0xx00000x

www.rsc.org/

Introduction

Functional organic molecules, especially their nanostructures (NS) usually possess excellent optical and electrical properties^{1,2} and have been widely applied in the fabrications of organic light-emitting diodes,^{3,4} organic field-effect transistors,⁵ and organic solar cell.⁶ Owing to the weak intermolecular forces (π - π conjugate, Van Der Waals force, H-bonds and charge-transfer interaction), the organic NS could offer many unique advantages such as the relative ease of chemical doping,^{7,8} good process ability,⁷ high reactivity⁹ and flexibility.¹⁰ These features make them the complementary to their inorganic counterparts. Although the modulations of the morphologies, optical and electrical properties have great significance for the better application of organic NS, much less progress has been achieved.

As a common organic semiconductor, perylene-3,4,9,10-tetracarboxylic dianhydride (PTCDA) combines the elements of perylene and peripherally rich oxygen atoms, which could favor the π - π conjugation between the layer-stacked molecules; and the excellent optical and electrical properties of PTCDA have attracted increasing attention and been extensively investigated in the past decades.¹¹⁻¹³ While the two-dimensional (2D) PTCDA films were prepared and studied

previously, the optical and electrical properties of PTCDA in confined geometries including nanorods (NRs), nanowires (NWs) or nanoparticles (NPs) still remain elusive.

Previously, a number of groups reported the synthesis of organic nanoneedles and NWs by the vapor phase deposition.¹⁴⁻¹⁶ Moreover, Zhao and co-workers have prepared the vertically aligned organic optical waveguide arrays of DAAQ on a silicon wafer at a proper temperature by the modification of the substrate surface both geometrically and chemically.^{17,18} A common view was that the preferred nucleation and growth of DAAQ NWs on high surface energy (E_s) sites made it possible to grow ordered arrays on prepatterned substrates.¹⁸

By the above analysis, the active sites with high E_s should be of great help for the preparations of organic NRs and NWs. In this study, porous anodic alumina oxide (AAO) was selected as the substrate to prepare PTCDA NS at different substrate temperature (T_s). As AAO is nearly transparent to visible light and possesses the excellent thermal and mechanical stabilities.¹⁹ Most importantly, the active sites with the smaller curvature radius on AAO surface are formed spontaneously during the anodizing processes, which possess high E_s and are expected to favor the nucleation of organic NS at the proper T_s .

Herein, we prepared film, NRs, NWs and NPs of PTCDA molecules and demonstrated the morphology modulation mechanism; then investigated the relationships between morphologies and optical properties of these NS in order to deeply understand the optical property modulation mechanism; finally, the electrical conductivity of a single-crystal NW was measured, which was found to be much higher than the conductivity of PTCDA film reported previously. These results are very promising for the potential applications of functional organic molecules.

^aHigh Magnetic Field Laboratory, Chinese Academy of Science, Hefei 230031, Anhui, People's Republic of China
E-mail: tianml@hmfl.ac.cn

^bNational Synchrotron Radiation Laboratory, School of Nuclear Science and Technology, University of Science and Technology of China, 42 Hezuohe Road, Hefei 230029, Anhui, People's Republic of China.
E-mail: fqxu@ustc.edu.cn

Electronic Supplementary Information (ESI) available: The fabrication process and the micro morphology of the AAO used as the substrates; Optical images of the AAO annealed and PTCDA NS formed on; SEM, TEM images and SAED patterns of the NRs and NWs forming on AAO at $T_s = 185$ and 275 °C; The cross-sectional SEM images of AAO that NPs formed on; The I - V curve of SiO_2 dielectric layer. See DOI: 10.1039/x0xx00000x

RESULTS AND DISCUSSION

Morphology and Growth Mechanism of PTCDA NS

Fig. 1(a) demonstrates the molecular structure of PTCDA, and Fig. 1 (b)-(f) present the images of scanning electron microscopy (SEM) of the NS formed on the AAO at different T_s . It was shown in Fig. 1(a) that PTCDA molecule combines the element of perylene, peripherally rich oxygen atoms and planar geometry, which could benefit the π - π conjugation between the layer-stacked molecules in different unit cell. From the SEM images in Fig. 1(b) and (c), which correspond to the samples prepared at $T_s = 50^\circ\text{C}$ and 110°C respectively, we noted that the PTCDA lumps formed and jointed together. These lumps constitute the PTCDA film that covered the majority of the porous cavities of the AAO. At the condition of $T_s = 50^\circ\text{C}$ and 110°C , the desorption of PTCDA molecules deposited on AAO is almost negligible, and therefore, forms the practically continuous film with the uniform thickness about 110 nm and 150 nm respectively. We also noted that the film thickness increases with the T_s increment from 50°C to 110°C . This result indicates the preferred vertical growth of the lumps. So the roughness of the film is enhanced as the T_s increases from 50°C to 110°C . The roughness enhancement of the PTCDA film with the T_s increment agrees with the previous results reported by A. J. Ferguson and T. S. Jones.²⁰

From Fig. 1(d), the short NRs were formed and dispersed evenly on AAO substrate at $T_s = 185^\circ\text{C}$. The length and width of the major NRs are about 350 nm and 130 nm respectively, as shown in the inset. And the major NRs locate at the pore openings with the hexagonal cross-section, indicative of the single-crystalline morphology (Fig. S3). The NRs nucleated at the pore openings and then grew outside the AAO pores. Therefore, the width of the NRs depends on the E_s or the curvature of the AAO surface.

Fig. 1(e) shows the NWs with the length about $5\ \mu\text{m}$ formed at $T_s = 275^\circ\text{C}$. The inset indicates that the NWs possess the square cross-section and are 70 nm wide approximately; furthermore, some short NRs were also formed. The formation of NWs and NRs closely relates with the induced nucleation effect on the active sites with high E_s . Previously, the higher E_s induced the preferred nucleation of the DAAQ NW were reported by Y. S. Zhao et al.¹⁷ At the given $T_s = 275^\circ\text{C}$, the areas with relative large curvature on AAO surface induce the preferable formation of initial nuclei, which possess large curvature and then grow epitaxially to form quasi one-dimensional (1D) single-crystal NWs with the large aspect ratio (Fig. S4). The areas with relative small curvature induce the laggard formation of initial nuclei with small curvature, and thus result in the formation of the NRs.

From Fig. 1(f), at the $T_s = 350^\circ\text{C}$, no NRs and NWs could be seen on the AAO surface. But we noticed from the enlarged image that many NPs (pointed by red arrows) with an average diameter of about 20 nm were formed at the pore openings of AAO. As the initial nucleus grow up to NPs, the curvature reduces correspondingly, and the $T_s = 350^\circ\text{C}$ is too higher to grow the PTCDA molecules epitaxially on the NPs. By carefully checking the corresponding images of the AAO cross section (see Fig. S5), some NPs were actually found inside the AAO pores.

Fig. 2 demonstrates the formation processes of PTCDA film, NWs, NRs and NPs, which illustrate the induced nucleation effect on the high E_s active sites of AAO. The representative active sites I, II, and III are indicated in Fig. 2, they are corresponding to the pore openings, the connection joints of three adjacent pores and the ridges of the two joint pores respectively. Firstly, the PTCDA molecules (represented by little red dots) were evaporated to the AAO surface. Then, at the lower $T_s = 50$ and 110°C , the PTCDA molecules deposited

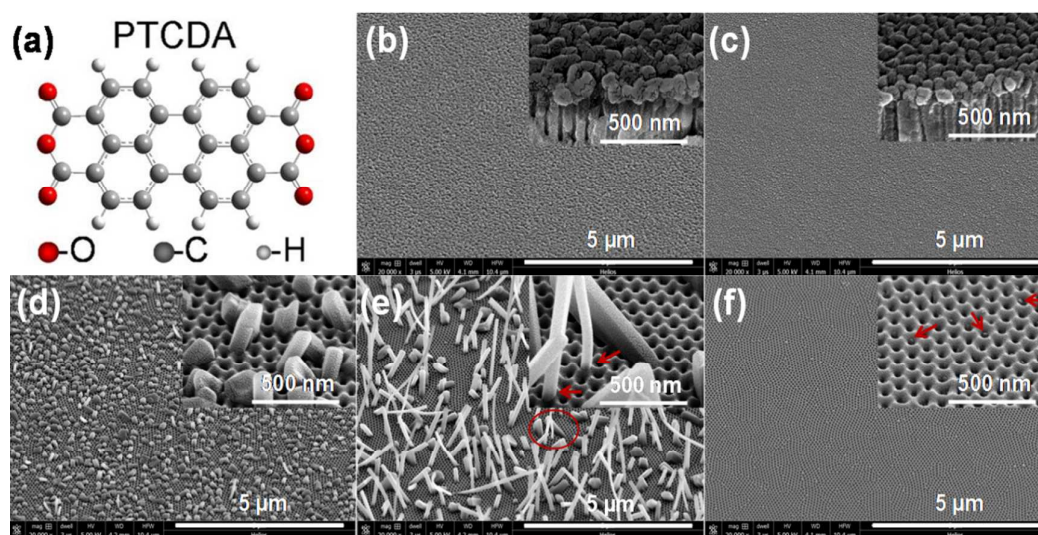


Fig. 1 Schematic structure of PTCDA molecule (a), and the NS of PTCDA formed on AAO at $T_s = 50^\circ\text{C}$ (b), 110°C (c), 185°C (d), 275°C (e), and 350°C (f) respectively. (The inset in each panel is the enlarged image, and three NPs are pointed by the red arrows. In order to visualize the morphology feature more clearly, the images were taken with a 45° tilted angle of the AAO surfaces)

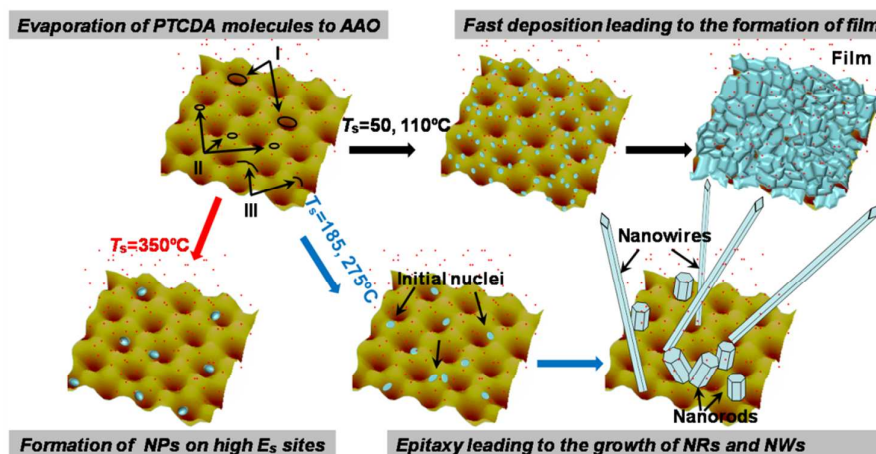


Fig. 2 Schematic illustration for the growth processes of PTCDA film, NRs, NWs and NPs.

and formed the little lumps on AAO surface, these lumps grew up and jointed together to constitute PTCDA film.

At the moderate $T_s = 185$ and 275°C , the PTCDA molecules deposited preferentially and formed the initial nuclei on the active sites. As the $T_s = 185^\circ\text{C}$, the PTCDA molecules deposited on the initial nuclei with the similar rate and form the short rods. As the T_s increases to 275°C , the PTCDA molecules epitaxially deposited slowly on the nuclei with the small curvature and grew to short NRs, but deposited quickly on the nuclei with the large curvature and grew to long NWs.

As the initial nuclei grew up, the curvature of the nuclei reduced (i.e., the E_s reduced) correspondingly. So, at $T_s = 350^\circ\text{C}$, once the nuclei grew to the NPs with the diameter about 20 nm, the PTCDA molecules could not deposited.

Optical Properties of PTCDA NS

In order to investigate the optical properties of NS with different morphologies formed on AAO, the UV-Vis absorption and PL characteristic spectra were measured.

Fig. 3(a) gives the UV-Vis absorption spectra of the AAO annealed and the NS prepared at different T_s . There is no

absorption band in the spectrum of the clean AAO, but the sharp feature at 556 nm (2.23 eV), a broad band near 479 ~ 471 nm (2.59 ~ 2.63 eV) and the two high energy bands at 374 nm (3.31 eV) and 358 nm (3.46 eV) appear as the PTCDA NS formed.

Previously, Jones et al. have investigated the effect of growth temperature on the photophysics of PTCDA thin film, and found that the absorption spectra of the films grown at different T_s were essentially identical, i.e., independent on the T_s .²⁰ Hoffmann et al. have investigated the Frenkel exciton (FE) and charge-transfer (CT) exciton in quasi one-dimensional organic crystal, and developed the charge-transfer-Frenkel mixing model to explain the absorption spectra of PTCDA crystal.²¹ According to the previous studies of Ferguson, Jones, and Hoffmann et al., the sharp feature at 2.23 eV originates from the CT dominated charge-transfer-Frenkel mixing mechanism (CT_{FE}) and the broad band near 2.59~2.63 eV comes from the FE dominated charge-transfer-Frenkel mixing mechanism (FE_{CT}).^{13,20,22} The two high energy bands at 3.31 and 3.46 eV arises from the intrinsic transition of PTCDA molecules. As the T_s increases, the lateral dimension of the NS

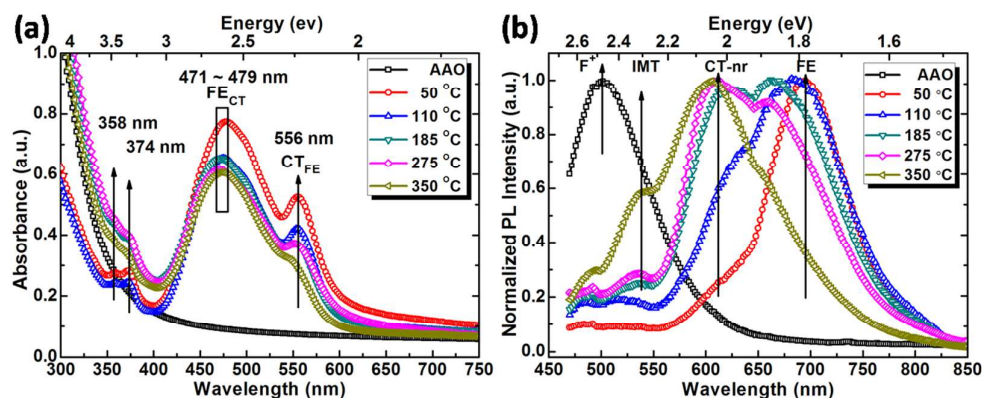


Fig. 3 (a) UV-Vis absorption and (b) PL spectra of the annealed AAO and the NS prepared at different T_s . (the excitation wavelength was 450 nm)

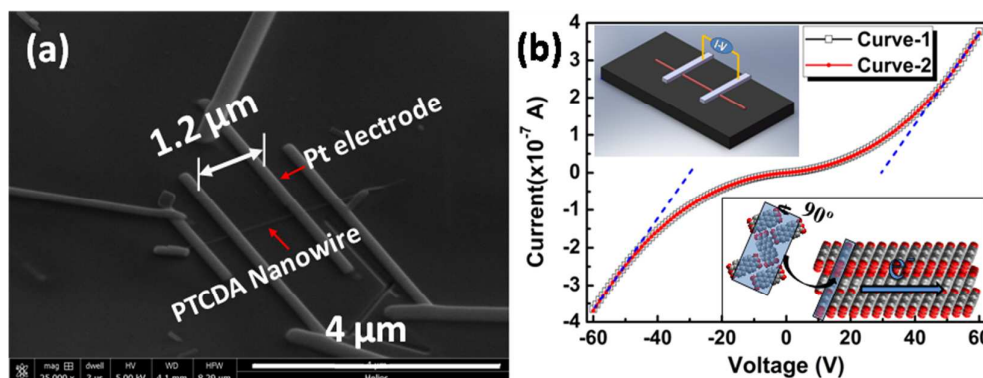


Fig. 4 (a) SEM image (45° tilted) of single NW as Pt stripes (width: 250 nm; thickness: 150 nm) acting as the electrodes, and the two inner Pt strips were used as the measuring electrodes. (b) the I - V curves measured by two-terminal technique, the up and down insets illustrate the measurement schematic and electron flow in PTCDA NW respectively.

decreases and results in the decrease of the intermolecular overlap degree, subsequently the broad absorption band shows the blue-shift effect. As the T_s increases, the positions of the other absorption peaks do not change significantly, only the absorbance decreases correspondingly. The UV-Vis absorption spectra show the similar characteristics as the previous reports on PTCDA thin film and α -PTCDA single crystals.^{13,20}

Fig. 3(b) gives the PL spectra of the AAO annealed and the NS prepared at different T_s . The PL intensities were normalized in order to stand out the emission intensity and position change. Only one emission band at 501 nm (2.48 eV), which originates from oxygen vacancy (F^+),²³ appears in the PL spectrum of the clean AAO, and the relative emission intensity reduces rapidly as the PTCDA NS formed. From Fig. 3(a) and (b), the emission band of AAO overlaps with the broad absorption band of PTCDA NS to a large extent; and the PTCDA molecules deposited by OMBD method will contact closely with AAO. Therefore, the energy matching and high quality interface between donor and acceptor are fulfilled for the Förster energy transfer. We conclude that there is a substantial energy transfer from oxygen vacancies (F^+) in AAO as the donor to PTCDA molecules in organic NS as the acceptor. From Fig. 3(b), the low energy emission plays the major role in the PL spectra of film, while the high energy emission is responsible for that of NRs, NWs and NPs with relative large specific surface areas.

To better understand the optical properties of PTCDA NS, we turn our attention to the modulation mechanism of the emission bands. In the previous reports by Wanger, the isolated monomer transition (IMT), the indirect FE transition, and the analogous non-relaxed charge transfer exciton (CT-nr) transition between the stacked molecules in different unit cells were used to explain the PL emissions of PTCDA single-crystals and film reasonably.^{13,22} Furthermore, the IMT comes from either the grain boundaries or the defects in PTCDA film and single-crystal. In this work, the PTCDA NS were prepared by the OMBD method in the ultra high vacuum (UHV) condition and especially the NRs and the NWs were single-crystal (Fig. S3 and S4), which reduced the defects concentration in NRs and

NWs effectively, so that the IMT transition mainly came from the single-crystal boundaries, i.e., the surface of NRs and NWs. According to SEM results, the specific surface area of the NS increases correspondingly as the T_s elevates from 50 °C to 350 °C. Consequently, the increase of T_s results in the enhancement of the IMT component in PL spectrum. So the high energy emission at about 2.30 eV is attributed to the IMT. In view of the blue shift of the PL band, the intermediate energy emission at about 2.05 eV and the low energy emission at about 1.85 eV arise from CT-nr transition and indirect FE transition respectively. Because the lateral dimension decrease of the NS results in the reduction of the intermolecular overlap degree, and thus induces the emission energies enhancement (i.e., blue shift) of CT-nr and FE transitions. There exist obvious differences in the PL spectra of PTCDA NS with different morphologies. This suggests that the PL properties are more sensitive to the NS morphology.

Electrical Property Measurement of PTCDA NW

Fig. 4 (a) gives the SEM image of the NW with the platinum (Pt) stripes acting as the electrodes which were deposited by the focus ions beam deposition (FIBD) techniques; the two inner Pt strips with the distance about 1.2 μ m were selected as the measuring electrodes. Fig. 4 (b) gives the current versus voltage (I - V) curves of the selected PTCDA NW, the up and down insets illustrate the measurement schematic and electron flow in PTCDA NW respectively. The two curves show the good repeatable performance. The electrical conductivity calculated according to the curve slope ($G = \Delta I / \Delta V \approx 1.21 \times 10^{-8}$ S) of the blue short dash lines (fitted curve in the I - V curve linear region) is about 3 ± 0.1 $S \cdot m^{-1}$, which is much higher than the conductivity of the PTCDA single crystal thin film without Ar^+ doping and comparable with the film doped by Ar^+ (dose $\sim 10^{15}/cm^2$) reported previously.²⁴ The relative higher electrical conductivity of PTCDA NW arises from both the strong π - π conjugation architecture between the high orderly arranged PTCDA molecules, which favors the charge carriers transfer perpendicularly to the layer-stacked PTCDA molecule planes, and the perfect crystalline structure of the single-

crystal NW, which effectively avoids the carriers scattering from defects.

Experimental

Preparation of PTCDA NS

The AAO prepared in 0.3 M oxalic acid solution at 40 V_{dc} were used as the substrates to prepare PTCDA NS, the detailed preparation process and micro morphology of AAO are given in the supporting information.

The preparations of PTCDA NS were carried out inside an UHV chamber by OMBD method. The AAO pretreated was transported into the UHV chamber and annealed at 360 °C in order to get the uniform properties of AAO and clean AAO surface. The vacuum recovery means the finish of the H₂O desorption and the oxalate decomposition. Next, the AAO annealed was cooled down to the selected T_s, and then the PTCDA powder was heated to the evaporation temperature (360 °C) and maintained for 5 min before the deposition. Five representative temperatures T_s = 50, 110, 185, 275, and 350 °C were selected to prepare the PTCDA NS. And the growth times were 90 min for all samples. The deposition rate of PTCDA molecules on the AAO at T_s = 50 °C was about 12.2 Å / min. The UHV base pressure was better than 5.0×10⁻¹⁰ torr and the working vacuum was maintained at ca. 5.0×10⁻⁸ torr during the deposition process. The evaporator was thoroughly degassed at 390 °C to remove the moisture and impurities contained in the as-purchased PTCDA powder (Aldrich).

Characterization of Optical Properties and Morphologies

The SEM images were obtained by FEI NanoLab 600i SEM/FIB dual beams system. The PL and UV-Vis absorption spectra were acquired using a Jobin Yvon Fluorolog-3-21 fluorescence spectrophotometer and a Shimadzu DUUV-3700 spectrophotometer respectively.

Fabrication of Device and Electrical conductivity Measurement of a single NW

The micro device was fabricated using FEI NanoLab 600i SEM/FIB dual beams system. The platinum (Pt) stripes (width: 250 nm; thickness: 150 nm) acting as the electrodes were deposited on a randomly selected PTCDA NW, which has been transferred previously onto a heavily doped Si substrate with a 300 nm SiO₂ layer. The I-V characteristics was carried out with table-top cryogenic probe station (Model TTPX) using a Keithley 2400 sourcemeter in vacuum (~10⁻⁵ torr).

Conclusions

In summary, film, NRs, NWs, and NPs of π-π conjugated PTCDA molecules were successfully prepared on AAO substrate by OMBD method. The NS morphologies can be modulated by the control of T_s. Only PTCDA film was prepared at T_s = 50 °C and 110 °C, as the PTCDA molecules deposited on everywhere of AAO surface with the almost equal probability

at the lower T_s; the NRs and NWs were formed at the medium T_s = 185 °C and 275 °C, and the lateral dimension tends to decrease as the T_s increases, because of the preferential formation of initial nuclei at the active sites with relative higher E_s and the epitaxial growth of these nuclei; merely NPs were generated when the T_s increased to 350 °C, as the T_s was so high that the PTCDA molecules could not deposit on the NPs. It was shown that the active sites with smaller curvature radius had the induced nucleation effect of PTCDA molecules. The specific surface area increase of PTCDA NS induced the enhanced emission of the IMT in PL spectra dramatically. The π-π conjugation degree between the layer-stacked PTCDA molecules decreased as the lateral dimension of NS reduced, which resulted in the CT-nr transition, the FE transition and the main absorption band shifted to high energy region. The I-V characteristic measurement illustrates that the PTCDA NW is a typical semiconductor and the electrical conductivity is about 3±0.1 S·m⁻¹. The relative higher electrical conductivity originates from both the strong π-π conjugation between the high orderly layer-stacked PTCDA molecules and the high crystallinity of PTCDA NW. These results should be of great significance for the better application of functional organic NS.

Acknowledgements

This work is financially supported by the National Natural Science Foundation of China (grant numbers: 11174294, 11374302, U1232137, U1432251,).

Notes and references

- 1 Y. S. Zhao, H. Fu, A. Peng, Y. Ma, D. Xiao and J. Yao, *Advanced Materials*, 2008, **20**, 2859-2876.
- 2 S.-Y. Min, T.-S. Kim, Y. Lee, H. Cho, W. Xu and T.-W. Lee, *Small*, 2015, **11**, 45-62.
- 3 W. Ding, Y. Wang, H. Chen and S. Y. Chou, *Advanced Functional Materials*, 2014, **24**, 6329-6339.
- 4 W. Xu, J. Zhao, L. Qian, X. Han, L. Wu, W. Wu, M. Song, L. Zhou, W. Su, C. Wang, S. Nie and Z. Cui, *Nanoscale*, 2014, **6**, 1589-1595.
- 5 B. J. Kim, Y. Ko, J. H. Cho and J. Cho, *Small*, 2013, **9**, 3784-3791.
- 6 P. A. Troshin and N. Serdar Sariciftci, in *Organic Nanomaterials*, John Wiley & Sons, Inc., 2013, DOI: 10.1002/9781118354377.ch25, pp. 549-578.
- 7 A. D. Peng, D. B. Xiao, Y. Ma, W. S. Yang and J. N. Yao, *Advanced Materials*, 2005, **17**, 2070-2073.
- 8 Y. S. Zhao, H. B. Fu, F. Q. Hu, A. D. Peng, W. S. Yang and J. N. Yao, *Advanced Materials*, 2008, **20**, 79-83.
- 9 S.-J. Lim, B.-K. An, S. D. Jung, M.-A. Chung and S. Y. Park, *Angewandte Chemie International Edition*, 2004, **43**, 6346-6350.
- 10 S. Kim, H.-J. Kwon, S. Lee, H. Shim, Y. Chun, W. Choi, J. Kwack, D. Han, M. Song, S. Kim, S. Mohammadi, I. Kee and S. Y. Lee, *Advanced Materials*, 2011, **23**, 3511-3516.
- 11 S. Heutz, A. J. Ferguson, G. Rumbles and T. S. Jones, *Organic Electronics*, 2002, **3**, 119-127.
- 12 D. Y. Zang, F. F. So and S. R. Forrest, *Applied Physics Letters*, 1991, **59**, 823-825.
- 13 V. R. Gangilenka, L. V. Titova, L. M. Smith, H. P. Wagner, L. A. DeSilva, L. Gisslén and R. Scholz, *Physical Review B*, 2010, **81**, 155208.

ARTICLE

Journal Name

- 14 Y. S. Zhao, C. Di, W. Yang, G. Yu, Y. Liu and J. Yao, *Advanced Functional Materials*, 2006, **16**, 1985-1991.
- 15 J. W. Chung, B.-K. An, J. W. Kim, J.-J. Kim and S. Y. Park, *Chemical Communications*, 2008, DOI: 10.1039/B802749H, 2998-3000.
- 16 J. Ryu and C. B. Park, *Advanced Materials*, 2008, **20**, 3754-3758.
- 17 Y. S. Zhao, J. Wu and J. Huang, *Journal of the American Chemical Society*, 2009, **131**, 3158-3159.
- 18 Y. S. Zhao, P. Zhan, J. Kim, C. Sun and J. Huang, *ACS Nano*, 2010, **4**, 1630-1636.
- 19 L. Fernández-Romero, J. M. Montero-Moreno, E. Pellicer, F. Peiró, A. Cornet, J. R. Morante, M. Sarret and C. Müller, *Materials Chemistry and Physics*, 2008, **111**, 542-547.
- 20 A. J. Ferguson and T. S. Jones, *The Journal of Physical Chemistry B*, 2006, **110**, 6891-6898.
- 21 M. Hoffmann, K. Schmidt, T. Fritz, T. Hasche, V. M. Agranovich and K. Leo, *Chemical Physics*, 2000, **258**, 73-96.
- 22 H. P. Wagner, A. DeSilva and T. U. Kampen, *Physical Review B*, 2004, **70**, 235201.
- 23 Y. Du, W. L. Cai, C. M. Mo, J. Chen, L. D. Zhang and X. G. Zhu, *Applied Physics Letters*, 1999, **74**, 2951-2953.
- 24 S. R. Forrest, M. L. Kaplan, P. H. Schmidt, T. Venkatesan and A. J. Lovinger, *Applied Physics Letters*, 1982, **41**, 708-710.